Antiproton, positron, and electron imaging with a microchannel plate/phosphor detector

ALPHA Collaboration, G. B. Andresen,[1] W. Bertsche,[2] P. D. Bowe,[1] C. C. Bray,[3] E. Butler,[2] C. L. Cesar,[4] S. Chapman,[3] M. Charlton,[2] J. Fajans,[3] M. C. Fujiwara,[5] D. R. Gill,[5] J. S. Hangst,[1] W. N. Hardy,[6] R. S. Hayano,[7] M. E. Hayden,[8] A. J. Humphries,[2] R. Hydomako,[9] L. V. Jørgensen,[2] S. J. Kerrigan,[2] L. Kurchaninov,[5] R. Lambo,[4] N. Madsen,[2] P. Nolan,[10] K. Olchanski,[5] A. Olin,[5] A. P. Povilus,[3] P. Pusa,[10] E. Sarid,[11] S. Seif El Nasr,[6] D. M. Silveira,[7,12] J. W. Storey,[5] R. I. Thompson,[9] D. P. van der Werf,[2] and Y. Yamazaki[12]

[1]*Department of Physics and Astronomy, Aarhus University, DK-8000 Aarhus C, Denmark*
[2]*Department of Physics, Swansea University, Swansea SA2 8PP, United Kingdom*
[3]*Department of Physics, University of California at Berkeley, Berkeley, California 94720-7300, USA*
[4]*Instituto de Física, Universidade Federal de Rio de Janeiro, Rio de Janeiro 21941-972, Brazil*
[5]*TRIUMF, 4004 Wesbrook Mall, Vancouver, British Columbia V6T 2A3, Canada*
[6]*Department of Physics and Astronomy, University of British Columbia, Vancouver, British Columbia V6T 1Z4, Canada*
[7]*Department of Physics, University of Tokyo, Tokyo 113-0033, Japan*
[8]*Department of Physics, Simon Fraser University, Burnaby, British Columbia V5A 1S6, Canada*
[9]*Department of Physics and Astronomy, University of Calgary, Calgary, Alberta T2N 1N4, Canada*
[10]*Department of Physics, University of Liverpool, Liverpool L69 7ZE, United Kingdom*
[11]*Department of Physics, NRCN-Nuclear Research Center Negev, Beer Sheva IL-84190, Israel*
[12]*Atomic Physics Laboratory, RIKEN, Saitama 351-0198, Japan*

(Received 2 October 2009; accepted 2 November 2009; published online 1 December 2009)

A microchannel plate (MCP)/phosphor screen assembly has been used to destructively measure the radial profile of cold, confined antiprotons, electrons, and positrons in the ALPHA experiment, with the goal of using these trapped particles for antihydrogen creation and confinement. The response of the MCP to low energy (10–200 eV, <1 eV spread) antiproton extractions is compared to that of electrons and positrons. © *2009 American Institute of Physics.* [doi:10.1063/1.3266967]

I. INTRODUCTION

Microchannel plate (MCP)/phosphor screen based diagnostics have proved invaluable in studying the evolution of lepton plasmas in Penning–Malmberg traps.[1–3] The MCP is used as an imaging device by accelerating electrons into a phosphor screen. It can also be used as a low-background particle detector by measuring current drawn by the MCP during measurements. These diagnostics provide a radial profile of the trapped particles that enables one to infer information about the plasma.

Recently, cold-antiproton ($\bar{p}$) experiments at CERN have extended the use of this diagnostic to antiprotons.[4–7] In this paper, the ALPHA collaboration reports on the relative and absolute sensitivity of the MCP to leptons and $\bar{p}$'s and shows how the diagnostic can be used to find the line-integrated radial density profiles of the particles in our Penning–Malmberg trap. The goal of the ALPHA collaboration is to synthesize, trap, and study antihydrogen. Knowledge of these radial profiles is invaluable in the optimization of this process.

The implementation of this diagnostic in our experiment is complicated by several unusual factors. Space and thermal isolation requirements force us to place the MCP in the fringe field of our solenoid. As a result, the path the particles take while being extracted from the trap to the MCP is sensitive to the details of magnetic fringe fields as well as the energy and mass of the particles. Additionally, $\bar{p}$'s annihilate when striking the MCP; products from these annihilation events can cause additional emission of electrons from the MCP. Thus, the response of the MCP to $\bar{p}$'s is greater[8] than one would predict from protons of equivalent energy. This enhanced response has not previously been well characterized.

II. PLASMA EXTRACTION PROCEDURE

In the ALPHA apparatus, non-neutral plasmas are confined in a Penning–Malmberg trap.[9] The traps employ a large superconducting solenoid to generate a 1 T axial magnetic field homogeneous over 80 cm to one part in 10^3 in the trapping region. This magnetic field confines the particles radially. A series of annular electrodes are used to create axial electrostatic wells for axial confinement. Two pairs of correction coils can be used to adjust the tilt of the magnetic field over 60 cm in the trapping region. Neutral (antihydrogen) atom confinement is achieved by adding an Ioffe-type octupole plus mirror fields. These fields create a magnetic minimum in which antihydrogen atoms can, in principle, be trapped. However, for the majority of this paper, particle imaging is performed without inclusion of the transverse neutral-trapping magnetic fields to simplify the analysis of data.

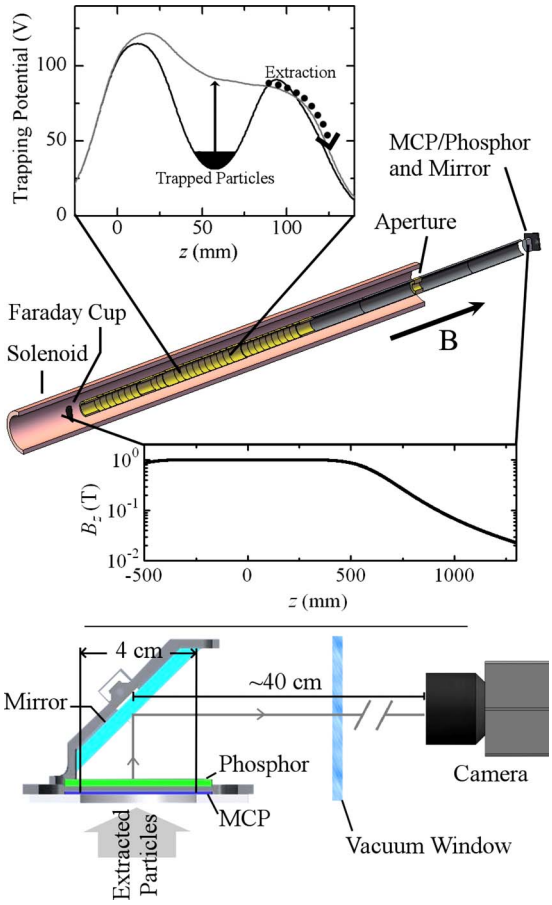

FIG. 1. (Color online) Cold plasma trap (top) and MCP imaging system (bottom) of the ALPHA experiment. Particles are extracted from the trap by slowly (over milliseconds) raising the potential under the trapped particles, allowing them to escape over the lower barrier of the well. Once over the barrier, the particles are ejected with an effective kinetic energy of 100 eV along the magnetic field. Particles that impact the MCP are amplified and imaged as described in the text.

An upstream injection line at CERN's antiproton decelerator facility provides antiprotons on average every ~100 s, some of which are degraded to ≤5 keV and captured.[10] Electron and positron sources are both located downstream from the trap. Once injected, the clouds of charges are manipulated into a desired location, density, and temperature through changes in electrode potentials, application of additional magnetic fields, and passive radiative cooling to the 7 K background temperature of the trapping environment.

To measure the plasma properties, the electrode potentials are manipulated so that the particles escape from the trap toward the MCP, which lies 1.3 m downstream from the trapping region, in the fringe region of the magnetic field (~240 G). (See Fig. 1.) Typically, particles are extracted from the trapping region with 100 ± 1 eV of energy. The plasma is highly magnetized during extraction, in the sense that particles follow magnetic field lines closely as they are constrained transversely by cyclotron motion. The magnetic field lines guide the extracted particles down the extraction column onto the MCP. The leptons are effectively bound to the field lines along their entire extraction trajectory; antiprotons deviate during the last few centimeters of their trajectory. This is discussed further in Sec. IV. The electrodes and aperture along the extraction column can collimate the outer edge of the particle cloud as it travels to the MCP, limiting the transverse size of the trapped particles we can image.

We image using a 4.0 cm diameter MCP and phosphor screen assembly purchased from El-Mul Technologies. The assembly is controlled by three voltages, applied to the front and back of the MCP and to the phosphor, that can be adjusted to suit the particle species and line density. The front voltage accelerates the incoming particles over the last few centimeters of their trajectories to a desired impact energy; this is usually set to give the particles a maximum impact energy of 200 eV. The MCP's back plate voltage relative to the front controls the gain of the MCP and is chosen to avoid saturation. The front-to-back voltage is varied from 900 V for low numbers of trapped particles ($N < 10^5$ leptons or 10^3 $\bar{p}$), down to 400 V for large numbers ($N > 10^8$ leptons or 10^5 $\bar{p}$). Higher gains (greater front-to-back voltages) saturate the MCP for large numbers of particles. We use a 120 ns response phosphor (P47) placed at 3.0 kV relative to the back of the MCP to convert the shower of electrons from the MCP to ~400 nm photons with an amplification factor α of 24 ± 3 photons/e^-.[11]

Images on the phosphor screen are captured on a charge coupled device (CCD) camera placed outside the vacuum chamber. The camera shutter is set to open over the entire extraction cycle. The CCD camera (PCO Sensicam QE) captures a 688×520 image from the phosphor screen with quantum efficiency $\eta_{qe}=40\%$ and signal readout resolution of ≈4.1 electrons (10.3 photons)/pixel on the CCD chip.[12] The area imaged by each pixel (6200 μm^2) is square and contains roughly 30 MCP channels. The cross section of photons that are measured on the CCD have an effective solid angle $\Omega_{cam}=2\pi(1-\sqrt{1-1/4N_f^2})$, where N_f is the f-number of the lens used with the camera. Putting this information together, the number of electrons stored on the CCD scales with the number charges emitted from the MCP by a factor $\eta_{qe}\alpha\,\Omega_{cam}/(4\ \pi)$. The ratio of electrons ejected from the back plate of the MCP to the number of incoming particles is referred to as the MCP's gain.

The large number MCP response to each species is calibrated by comparing the extractions of particles to the MCP to extractions to a Faraday cup held at 1 T, 40 cm upstream from the trap region. Since both measurements are destructive, they must be performed on successive injections of particles. For leptons, we find the results to be very repeatable, having reliable counts of particles with ≤5% injection variance during steady operation. The number of leptons is found by measuring the total accumulated charge on the Faraday cup, with a background noise level of 10^5 charges. However, this technique does not work for $\bar{p}$'s since there are significantly fewer of them, and the resulting signal is below the noise level of our electronics. Additionally, even if the noise level was improved, the accumulated charge would not directly indicate the $\bar{p}$ number since decay products from nuclear-$\bar{p}$ annihilations may carry away charge. Instead, the Faraday cup is utilized as a beam stop, and $\bar{p}$ numbers are found by detection of charged particles from annihilations on the Faraday cup by nearby scintillator/photomultiplier pads.

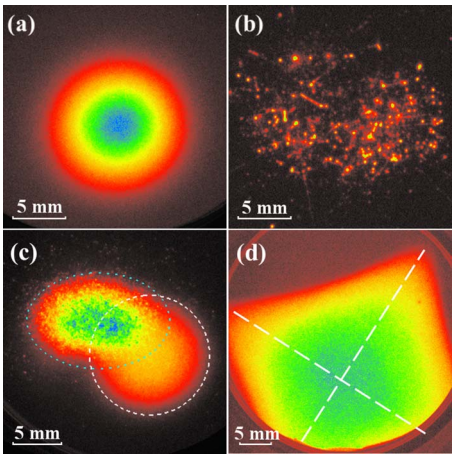

FIG. 2. (Color online) In (a), we show a typical profile of a lepton plasma; in this case, positrons. The high-gain, sparse $\bar{p}$ image in (b) shows the tracks from annihilation products of the antiprotons. During a mixing operation (c), overlapping e^- (white dash) and $\bar{p}$ (cyan dots) are extracted simultaneously to demonstrate differences in the transverse mapping of species. Note that $\bar{p}$'s make defined speckled patterns while the electrons image to a smoother distribution due to the number of particles imaged ($\sim 10^6$ e^- and $\sim 10^4$ $\bar{p}$). Perturbing the extraction with transverse trapping fields (octupole) produces images with azimuthally dependent deformation as shown in (d); axes of deformation are shown as white, dashed curves. Color intensity (red to blue) scales to the peak intensity of each image.

The efficiency for $\bar{p}$ annihilation detection by the scintillator/photomultiplier tube system is estimated by Monte Carlo simulations to be $25 \pm 10\%$. The accuracy is in part limited by the knowledge of the branching ratios of annihilation reactions. Since this is an unknown of the overall scaling factor, and is not apparent in measurements, we have chosen to omit this uncertainty in figures in this paper with the understanding that it is always present for absolute $\bar{p}$ numbers.

III. MCP CALIBRATION

MCPs consist of a dense array of amplifying channels. Particles that hit the front of the MCP may release electrons into a channel.[13] The electron is accelerated along the channel, and may initiate a cascade within the channel. For a small number of particles, the MCP gain may be as high as 3×10^4 (for leptons); however, if a large number of particles is extracted, we find that the gain is more limited. This happens because the rate at which charge is expelled from each channel during measurement is much greater than the current from the circuit's *RC* recovery, effectively depleting the channel.[14] We measured the stored charge limit to be $\sim 2 \times 10^4$ electrons on average per MCP channel.

The impact of one low energy electron or positron initiates approximately one cascade. An antiproton, however, annihilates with the MCP material. The high energy secondary particles that result from the annihilation can excite additional cascades, enhancing the MCP gain. Tracks from secondary particles are often visible in images taken with our MCP, as shown in Fig. 2(b). Thus, the response of the MCP to individual $\bar{p}$'s varies. Using images similar to Fig. 2(b), with low numbers of extracted particles, we compare the distribution of the spot intensities on the phosphor screen from both electrons and antiprotons in Fig. 3. When necessary, we take care to aggregate the signal from a $\bar{p}$ spot and its track. We find that the response per $\bar{p}$ event has a much wider distribution than for the electrons. Despite the wide distribution in intensities of an individual event, the data shown in Fig. 4 demonstrate that, experimentally, the MCP response to a cloud of $\bar{p}$'s is linear over a wide and useful regime. Profiles for a small number of events can still be generated by point-finding routines on the image. The measurements in Figs. 3 and 4 were taken at the maximum MCP gain settings to demonstrate that the detector does not saturate for the number of $\bar{p}$'s measured.

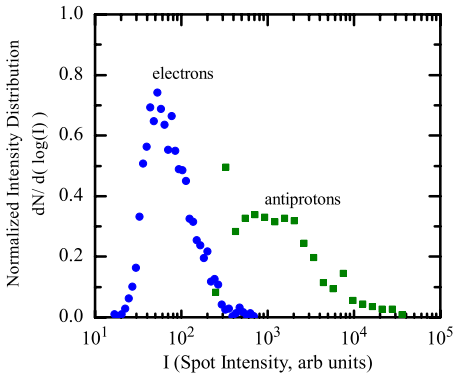

FIG. 3. (Color online) Normalized $[\lim_{I \to \infty} N(\log I) = 1]$ electron and antiproton spot intensity distributions. For both species, the MCP front-to-back voltage was 900 V; the impact energy was 200 eV. These parameters maximize the gain.

Figure 5(a) compares the MCP response to $\bar{p}$ and leptons as a function of front-to-back bias. The data were obtained by extracting the particles from the trapping region with a uniform energy of 100 eV and then varying the impact energy by changing the bias on the front plate of the MCP. This procedure assures that extraction energy and trajectories are independent of the bias as the potentials are largely identical over all but the last few centimeters of the particle paths. Since we assume that branching ratios of nuclear-$\bar{p}$ annihilation do not change significantly for low impact energies, the supposition that the response is generated from $\bar{p}$ annihilation products of $\bar{p}$ implies that the effective gain should be largely independent of $\bar{p}$ impact energy. However, the method of changing the bias of the front plate of the MCP to adjust impact energy has an additional effect on the gain. For $\bar{p}$ impact energies of less than 100 eV, the absolute bias on

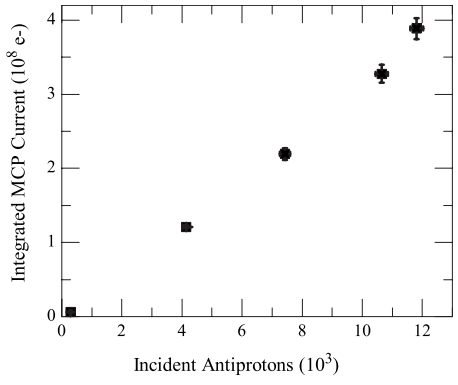

FIG. 4. Response of the MCP as a function of the number of $\bar{p}$. Same biasing parameters as in Fig. 3.

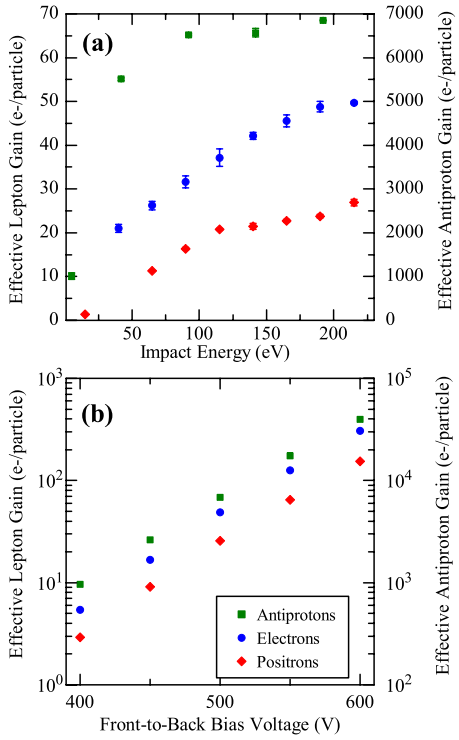

FIG. 5. (Color online) Effective gain of the MCP for different species of particles while varying the voltages on the front and back plates. Particles are extracted from the trap at ~100 eV and accelerated by the front plate voltage. In (a), the front-to-back voltage bias was kept constant at 500 V, while impact energy is varied; in (b), the front-to-back voltage bias is varied while the impact energy is held at 200 eV. The uncertainties in the measurements in (b) are <2%.

the MCP front plate is negative; this can reduce the measured gain, since electrons ejected off the front plate are pushed out to the grounded walls of the vacuum chamber instead of being pulled back onto the MCP. We are unable to disentangle this effect from the response of the detector for low energy $\bar{p}$ impacts. This effect manifests itself for leptons as well; the kink near 100 eV in the e^+ response occurs because the front bias is repulsive to secondaries for impact energies of greater than 100 eV (since the e^+ charge is opposite of the $\bar{p}$ and e^-).

The gain for all three species of particles increases near exponentially with the front-to-back bias, as shown in Fig. 5(b). This result indicates that the underlying amplification mechanism of the MCP remains intact, despite a two order-of-magnitude difference in the gain response. We do not expect the 240 G magnetic field on the MCP to greatly affect the gain from a zero field setting since the length scale of electron cyclotron motion in the channel is much larger than the channel size on the MCP. However, this might no longer be the case if the MCP were placed in fields on the order of 1 T.

IV. RADIAL PROFILE

The mapping between the observed radial profile and the actual plasma can be quickly constructed under the assumption that the particles are strongly magnetized, meaning the distance traveled during a cyclotron period satisfies $v_\parallel/\Omega_c \ll |(\partial \mathbf{B}/\partial z)/B|^{-1}$, where $v_\parallel$ is the transverse velocity and Ω_c is the cyclotron frequency. When this assumption is met, charged particles closely follow field lines onto the MCP, leading to a radial expansion of $\sqrt{B_{\mathrm{trap}}/B_{\mathrm{MCP}}}$ about the axis of the solenoid. Simulations using a fourth-order Runge–Kutta trajectory solver find that magnetic guiding overestimates the expansion by 2 % for antiprotons; electrons remain strongly bound to field lines and the expansion is accurately predicted by the above estimate.

Even strongly magnetized particles will undergo $\mathbf{E}\times\mathbf{B}$ and magnetic curvature drifts. In our system, drift corrections are on the order of ~100 mrad about the magnetic trap axis during the extraction process from the trapping region to the MCP. Since electrons and positrons are ejected from the trap with much higher velocities, and in much greater densities than the antiprotons, the drifts induce species-dependent rotations of the MCP image from the actual trapped particle distribution. These differences would not be noticeable for radially symmetric plasmas since the drifts would induce azimuthal motion; however, misalignments between the magnetic field lines and the electrode axis can drive these rotations about an "off-center" axis. We observe offsets, shown in Fig. 2(c), between $\bar{p}$ and lepton images, that we attribute to this effect.

To simplify our interpretation of images, we normally extract particles with the transverse neutral trapping fields turned off. However, when particles are ejected in the presence of such transverse multipole fields, the magnetic field lines, and therefore the trajectories become more complex. A distorted image [Fig. 2(d)] generated by the inclusion of magnetic fields for neutral particle transverse-confinement is observed with octupole symmetry as expected. Knowing the applied multipole moments, the radial profile can, in principle, be reconstructed from such images by applying an appropriate mapping of the field lines back into the trapping region.

V. CONCLUSION

We have developed an MCP/phosphor screen system to measure the radial distribution of low energy electrons, positrons, and antiprotons extracted from a Penning trap. We have calibrated the response of the MCP to all three species and found that the gain for antiprotons is significantly higher than the gain for leptons. We posit that this behavior is due to additional MCP channels being triggered by nuclear-$\bar{p}$ annihilation products.

ACKNOWLEDGMENTS

This work was supported by CNPq, FINEP (Brazil), ISF (Israel), MEXT (Japan), FNU (Denmark), NSERC, NRC/TRIUMF (Canada), DOE (USA), and EPSRC and the Leverhulme Trust (U.K.).

[1] D. Durkin and J. Fajans, Phys. Fluids **12**, 289 (2000).
[2] J.-H. Choi, B. Knuffman, X. H. Zhang, A. P. Povilus, and G. Raithel, Phys. Rev. Lett. **100**, 175002 (2008).
[3] A. J. Peurrung and J. Fajans, Rev. Sci. Instrum. **64**, 52 (1993).
[4] H. Higaki, N. Kuroda, K. Y. Franzen, Z. Wang, M. Hori, A. Mohri, K. Komaki, and Y. Yamazaki, Phys. Rev. E **70**, 026501 (2004).
[5] G. Andresen, W. Bertsche, A. Boston, P. D. Bowe, C. L. Cesar, S. Chapman, M. Charlton, M. Chartier, A. Deutsch, J. Fajans, M. C. Fujiwara, R.

Funakoshi, D. R. Gill, K. Gomberoff, J. S. Hangst, R. S. Hayano, R. Hydomako, M. J. Jenkins, L. V. Jørgensen, L. Kurchaninov, N. Madsen, P. Nolan, K. Olchanski, A. Olin, A. Povilus, F. Robicheaux, E. Sarid, D. M. Silveira, J. W. Storey, H. H. Telle, R. I. Thompson, D. P. van der Werf, J. S. Wurtele, and Y. Yamazaki, Phys. Rev. Lett. **98**, 023402 (2007).

[6] G. Andresen, W. Bertsche, P. D. Bowe, C. C. Bray, E. Butler, C. L. Cesar, S. Chapman, M. Charlton, J. Fajans, M. C. Fujiwara, R. Funakoshi, D. R. Gill, J. S. Hangst, W. N. Hardy, R. S. Hayano, M. E. Hayden, R. Hydomako, M. J. Jenkins, L. V. Jørgensen, L. Kurchaninov, R. Lambo, N. Madsen, P. Nolan, K. Olchanski, A. Olin, A. Povilus, P. Pusa, F. Robicheaux, E. Sarid, S. Seif El Nasr, D. M. Silveira, J. W. Storey, R. I. Thompson, D. P. van der Werf, J. S. Wurtele, and Y. Yamazaki, Phys. Rev. Lett. **100**, 203401 (2008).

[7] G. Andresen, W. Bertsche, P. D. Bowe, C. C. Bray, E. Butler, C. L. Cesar, S. Chapman, M. Charlton, J. Fajans, M. C. Fujiwara, R. Funakoshi, D. R. Gill, J. S. Hangst, W. N. Hardy, R. S. Hayano, M. E. Hayden, A. J. Humphries, R. Hydomako, M. J. Jenkins, L. V. Jørgensen, L. Kurchaninov, R. Lambo, N. Madsen, P. Nolan, K. Olchanski, A. Olin, R. D. Page, A. Povilus, P. Pusa, F. Robicheaux, E. Sarid, S. Seif El Nasr, D. M. Silveira, J. W. Storey, R. I. Thompson, D. P. van der Werf, J. S. Wurtele, and Y. Yamazaki, Phys. Plasmas **15**, 032107 (2008).

[8] M. H. Holzscheiter, R. E. Brown, J. B. Camp, S. Cornford, T. Darling, P. Dyer, T. Goldman, S. Høibråten, K. Hosea, R. J. Hughes, N. Jarmie, R. A. Kenefick, N. S. P. King, D. C. Lizon, M. M. Nieto, M. M. Midzor, S. P. Parry, J. Rochet, R. A. Ristinen, M. M. Schauer, J. A. Schecker, and F. C. Witteborn, Nucl. Phys. A **558**, 709 (1993).

[9] W. Bertsche, A. Boston, P. D. Bowe, C. L. Cesar, S. Chapman, M. Charlton, M. Chartier, A. Deutsch, J. Fajans, M. C. Fujiwara, R. Funakoshi, D. Gill, K. Gomberoff, D. Grote, J. S. Hangst, R. S. Hayano, M. Jenkins, L. V. Jørgensen, N. Madsen, D. Miranda, P. Nolan, K. Ochanski, A. Olin, R. D. Page, L. G. C. Posada, F. Robicheaux, E. Sarid, H. H. Telle, J.-L. Vay, J. Wurtele, D. P. van der Werf, and Y. Yamazaki, in *Low Energy Antiproton Physics*, edited by D. Grzonka, R. Czyzykiewicz, W. Oelert, T. Rozek, and P. Winter (AIP, New York, 2005), Vol. 796, p. 301.

[10] G. Andresen, W. Bertsche, A. Boston, P. D. Bowe, C. L. Cesar, S. Chapman, M. Charlton, M. Chartier, A. Deutsch, J. Fajans, M. C. Fujiwara, R. Funakoshi, D. R. Gill, K. Gomberoff, R. S. Hayano, R. Hydomako, M. J. Jenkins, L. V. Jørgensen, L. Kurchaninov, N. Madsen, P. Nolan, K. Olchanski, A. Olin, R. D. Page, A. Povilus, F. Robicheaux, E. Sarid, D. M. Silveira, J. W. Storey, R. I. Thompson, D. P. van der Werf, J. S. Wurtele, and Y. Yamazaki, J. Phys. B **41**, 011001 (2008).

[11] ScintiMax Spec, sheet, 2007, http://www.el-mul. com/My%20Documents/pdf/ScintiMax_2007.pdf.

[12] Sensicam qe datasheet, http://www.pco.de/fileadmin/user_upload/db/products/datasheet/sensicam_qe_20080624.pdf.

[13] J. L. Wiza, Nucl. Instrum. Methods **162**, 587 (1979).

[14] G. W. Fraser, M. T. Pain, J. E. Lees, and J. F. Pearson, Nucl. Instrum. Methods Phys. Res. A **306**, 247 (1991).